Large Enhancement of Mechanical Properties and Environmental Resistance of Glass Fibre from Polymer Coating with Low Fraction of Nano-reinforcements

S.L Gao, E. Mäder, and R. Plonka

Leibniz Institute of Polymer Research Dresden, Hohe Str. 6, 01069 Dresden, Germany,
gao@ipfdd.de, emaeder@ipfdd.de, plonka@ipfdd.de

ABSTRACT

The severe surface flaws of brittle materials can be 'healed' using coating. Here, we describe an inexpensive and applicable process by which a nanometer-scale polymer coating layer based on styrene butadiene with varied mutiwalled carbon nanotubes (MWCNTs) and/or nanoclays, as environmental barrier coating layer, was applied to alkali-resistant glass (ARG) fibres. Our data indicates that the nanostructuring functionalised glass fibre shows significantly improved both mechanical properties and corrosion resistance to alkali. Moreover, the mechanisms of enhanced mechanical properties and environmental resistance are discussed and an assessment of changes in the fibre surface nanomechanical properties is provided.

Keywords: nanocoatings, clays, nanotubes, alkali-resistance glass fibre, nanoindentation

1 INTRODUCTION

Surface defects of brittle materials acting as tiny pre-existing cracks can propagate through the material to cause fracture, resulting actual tensile strength much lower than the corresponding theoretical strength. The nanoscale surface defects providing extra stress at the tip of the cracks can lead to stress-corrosion cracking at low stress level, particularly in a humid environment. Surface coatings are believed efficiently to protect the fibre surface against alkali/acidic/moisture and thus to improve fibre's mechanical properties. Recently, we applied a styrene–butadiene coating on alkali-resistant glass (ARG) fibre surface as environmental barrier layer which buffer the alkaline groups of the cementitious matrix and show significantly improved corrosion resistance to alkali [1]. The mechanical 'healing' effect was also viewed as a disappearance of the severe surface flaws because of an increase of the crack tip radius, the flaw filled by coating being either elliptical than sharp [2]. Molecular dynamics simulations show that the stress concentration at the notch tip is significantly reduced due to the presence of the nanoparticles [3]. We found it interesting to observe that the tensile strength of ARG and E-glass fibres can be well described by bimodal Weibull cumulative distribution function for different sizing systems [4]. The application of nanocomposite coatings locally at the fibre surface could potentially yield both surface defect-free and functionalised interfaces that exhibit enhanced mechanical properties and environmental durability.

Here we further reinforce traditional glass fibres using different nanostructured coating layers with nanotubes and/or organoclay, to provide a protective layer against physical/chemical damage. Fundamentally, nanostructuring surface is motivated by the grace and efficiency of natural materials, in a biomimetics approach. It is evolved in these materials as shown in Fig.1 that multiscale structures (i.e. bones) and skin coverings with a flexible layer of overlapping tough scales (vertebrates, i.e. fishes), mainly composed of nanostructured insoluble protein keratin and minerals. It was believed that the nanometer size of mineral particles ensure optimum strength and maximum tolerance of flaws [5]. As the structural size shrinks to the nanometer scale, there is a transition of fracture mechanism from the classical Griffith LEFM to one of homogeneous failure with no stress concentration at the crack tip [6]. The surface free energy becomes more dominant and the material strength is limited by theoretical strength of solid and the structure becomes insensitive to pre-existing flaw. In the case of man-made materials such as carbon nanotubes, their high Young's modulus and tensile strength makes them ideal candidates as reinforcements for structural composites. In this work, traditional glass fibres were covered using nanoscale coating layers with multi-walled carbon nanotubes (MWCNTs) and/or layered clay silicates (Fig.1 right).

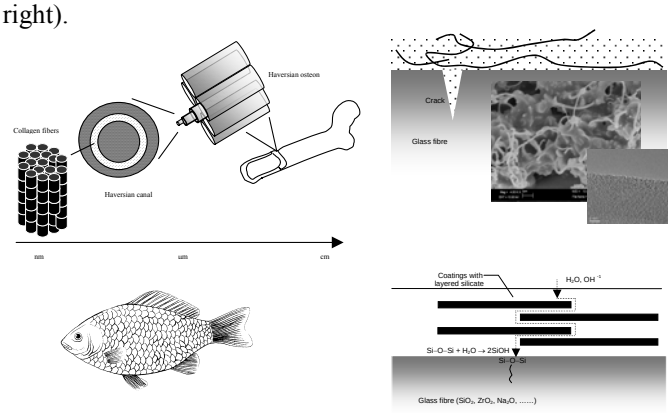

Figure1: Natural strategy and application of nanostructed coating. Examples of mechanical reinforcement and environmental resistance by multi-scale fibres and overlapping tough scales (left), applications of coatings with nanotube/layered silicate polymer network on glass fibre surface to enhance flaw 'healing' effect and corrosion resistance (right). The inserts show polymer/MWCNT network and individual nanotube's structure.

2 METHODS

The control fibres utilized in this work were ARG-IPF fibres with diameter of 17 μm, made at Leibniz Institute of Polymer Research Dresden. During the continuous spinning process, the ARG fibres were sized by an alkali resistant sizing consisting of silane coupling agent, γ–APS, in conjunction with film formers and nanoparticles in the aqueous sizing. We applied surface coatings based on styrene-butadiene copolymer to the control ARG-IPF fibres. The 1 wt% MWCNTs (IFW, Germany) are dispersed in the epoxy resin based solution. The organo-clay particles (Nanofil 15, Süd-Chemie AG, Moosburg, Germany) in maleic anhydride grafted polypropylene with an average size of 65 to 130 nm is dispersed in the obtained solution. A quaternary ammonium surfactant and a non-ionic surface active agent were added to the dispersion for homogeneous distribution of the constituents with or without 1 wt% clays. The total weight gain due to the coating is 5.3 wt% measured by pyrolysis (600°C, 60 min) of the coated fibres. We extracted the fibres in selected highly concentrated aqueous alkaline solution (5 wt % NaOH, pH of 13) at 20 ^{o}C for seven days, which is the most aggressive and corrosive condition to the fibre surface [4].

The single fibre tensile measurement was conducted under 65±2 % RH and 20±2 °C using the Fafegraph ME testing device (Fa. Textechno) equipped with a 100 cN force cell. The cross head velocity is 10 mm/min and the gauge length is 20 mm in accordance with EN ISO 5079. Based on a vibration approach, the fineness of each selected fibre was determined by using a Vibromat ME (Fa. Textechno) in accordance with EN ISO 53812 and ASTM D 1577. An AFM (a Digital Instruments D3100, USA) was used as both a surface imaging tool and a nanoindentation device for measuring contact stiffness and modulus. The topography and phase images of samples were studied in tapping mode. The cantilever (ULTRASHARP NSC15-F/5, MikroMasch, Estonia) has a normal spring constant of 40.9 N/m, a tip cone angle of 20^{o}, radius of ~10 nm and modulus of 160 GPa to assure good imaging resolution and nanometer scale indents.

3 RESULTS AND DISCUSSION

We have shown previously that the critical flaws which limited the strength of these fibres were located at the surface. The fibre fracture behaviour is strongly affected by the variation of coating properties in terms of thickness, roughness and mechanical properties as well as the distribution and fraction of nanotubes. Here, we show that the tensile strength of surface nanostructured ARG fibres with both nanotubes and organoclay are significantly improved (Fig. 2). At MWCNTs loading of only 1 wt% in the coatings, the fibre strength improved by 70 %, while the strength improved by 25 % in the coated fibre with an organoclay loading of 1 wt%**.** Interestingly, both the Weibull plot lines and modulus of coated systems shift to higher values than those of the control, indicating reduction of size of strength-controlling surface defects and defects with lower heterogeneity distribution. In other words, it indicates that the coatings heal the surface flaws, which in turn show similar severity and therefore flaw homogeneity relative to the control fibres. The effects of alkali attacks on the average fibre strength are also compared in Fig. 2. Importantly, the durability and alkali-resistance are also improved, particularly the fibre with organoclay coating. It is evident that sample of clay coatings would not yield an evident strength reduction upon treatment. However, the strength reduction for systems with nanotube coatings occurred. An additional coating C2 resulted in marginal improvement of alkali resistance. Nevertheless, the coated fibres have higher strength values than the control one after akali corrosion, reflecting the improved environmental durability for fibres with nanostructuring coatings.

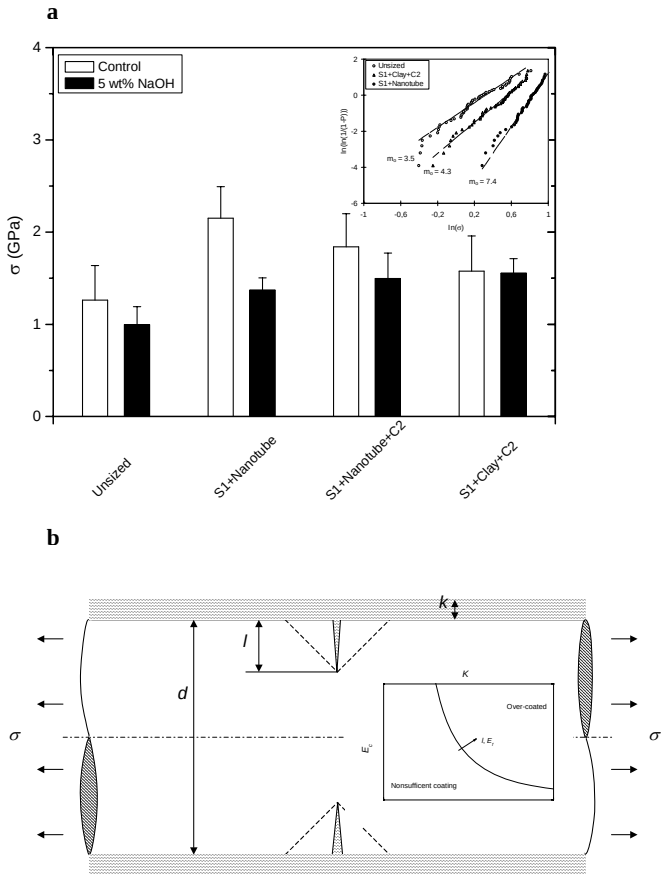

Figure 2: Dependence of mechanical properties and corrosion resistance on AR fibre surface coating. a, Effect of the nanostructed coating with low fraction nanoreinforcements on the tensile strength of ARG fibre before and after alkali treatment. The insert shows Weibull plot of fibre fracture probability. b, A coated fibre with a surface flaw. The insert shows optimistic heal condition of coatings.

Potential mechanisms of this mechanical property improvements include the contributions of different factors, i.e. coating layer and nanoclay plates preventing moisture/alkali contact and reaction with glass lattice at a

crack tip (stress corrosion); crack tip filled by resin/nanoparticles reducing stress concentration; stress-redistribution and crack stopping mechanisms by coating and nanotube's 'bridging' effect and interface debonding/plastic deformation around crack tip; compressive stress on fibre surface preventing crack opening/propagation by the shrinkage of polymer solidification, et al. To simplify the complex phenomena, we developed a simple mechanical model based on Griffith fracture mechanics to estimate the strength of coated fibre. Consider a coated fibre loaded in tension and having a thin circumferential crack as shown in Fig. 2b. The crack length, l, is much less than the fibre diameter, d. When the crack appears, the strain energy is released in a material volume adjacent to the crack. Assume that this volume is comprised by a conical ring whose generating lines are shown by broken lines and heights are proportional to the crack length. On the other hand, formation of new surfaces and failure of coating consume the energy. According to the energy balance, the coated fibre strength, σ_f, can be expressed as

$$\sigma_f > \overline{\sigma}_f = \sqrt{\frac{2\gamma E_f}{(\beta l - k\frac{E_c}{E_f})}} \quad (1)$$

where γ is surface energy and β is a constant coefficient of proportionality. E_f and E_c are Young's modulus of fibre and coatings, respectively. Notably, the critical tensile stress of fibre with surface flaw, $\overline{\sigma}_f$, is significantly affected by the coating modulus and thickness. The thicker the coating layer and stiffer the stiffness of coating the higher is the tensile strength of the fibre. On the other hand, the larger the size of defect and stiffer the stiffness of fibre and the thicker and stiffer the coatings are required for effective repairing (Fig.2b). Equation 1 implies that the highest strength can be achieved for fibre with surface defect when the coatings have $kE_c \geq \beta l E_f$, that is to say, the equation and associated assumptions are not valid. The model allows us to estimate the coating stiffness based on the tensile strength of fibre as

$$E_c = \frac{2\gamma E_f^2}{k}\left(\frac{1}{\sigma_0^2} - \frac{1}{\sigma_f^2}\right) \quad (2)$$

where σ_o is strength of fibre without coating. Taking a rough estimate $\gamma = 3.5$ J/m^2 for glass, $E_f = 70$ GPa, and $k = 1$ μm, we can calculate the modulus of coatings, E_c to be ≈ 14 GPa for nanotube coating and ≈ 8 GPa for clay coating, respectively. Interestingly, it is a fairly good agreement with the values of 17 GPa and 9 GPa for the two corresponding nanocomposite systems calculated by rule of mixture (ROM) in a parallel model.

We then examined whether the dispersed organoclay was intercalated or exfoliated in the coatings. Individual crystallites observed by AFM (Fig.3a) display the lath-type morphology of hectorite. The measured height of individual particles equals ~ 1.5 nm, which corresponds to the thickness of one single smectite layer. Fig. 3b shows that the fracture surface topography of coating film with clays after alkali treatment consists of many similar shape particles. Random distribution of the particles dispersed in the coating polymer matrix is clearly visible. Consisting of a layered structure of aluminum sandwiched between two layers of silicon, these clays provide high surface areas of contact between the platelet and the polymer matrix. Obviously an appreciable level of platelet content and orientation is required to provide a significant alkali barrier enhancement. It is clear that the silicate layers of clay are intercalated because the measured stacked intercalated silicate layers have a thickness of ~ 6 nm and lateral size of 80 nm. Besides measuring surface topography, images of other surface physical properties such as contact stiffness (hardness) and adhesion are measurable with the AFM. Fig. 3c and d show the topography images and corresponding contact stiffness image of the pyrolysed fibre surface where the polymer was removed and clay particles remained. The stiffness image were determined by nanoindentation in force volume mode of AFM, in which an array of nanoindentation force-displacement curves were measured across the sample surface at regular intervals with a constant maximum indentation force. The stiffness map was plotted as a grey-scale image, with lighter shades representing deeper indentation depth, in other words, lower contact stiffness. Worth noting is that no apparent difference of the stiffness and surface adhesion force was found between glass fibre and clay particles which exhibit a very similar response to the indentation tip.

To determine how the fibre morphologies are altered on a microscopic level by the concentrated alkaline environmental attacks, we observed fibre surface and stiffness (Fig. 4). The fairly smooth and featureless surface of control (unsized) sample presents no apparent height differences (Fig. 4a), while the coated fibres with or without clays show the thin and thick coating layer with irregular distribution in all three dimensions (Fig. 4b,c). It is interesting to note that the coated fibre with clays has similar surface features before and after extraction, which indicates the coating layer not being fully removed. In contrast, both the control and coated fibres without clay had a microrough porous surface morphology with particles cover the surface after extraction. It seems that not only most of the coating is removed but also the most top layer of glass is chemically corroded. Our nanoindentation tests provide an indication of the variability of the local contact stiffness of the fibre surface (see Fig. 4f). It is evident that surface stiffness within indentation depth (< 6 nm) was strongly affected by coating nature and alkali extraction. We plotted the best-fit lines of experimental data in Fig. 4f, giving the fibre surface moduli of 9.0 GPa and 7.8 GPa for the coating and coating with clay systems, respectively, which is surprisingly close to the calculated coating modulus by above equation because the data arised from different test and stress conditions. After alkali treatment, the surface moduli of the coating and coating with clay specimen either increases to 30.7 GPa or decreases to 3.9 GPa, respectively. In conjunction with above topographic

imaging observation in the case of fibre with coatings (Fig. 4b), the increase of surface stiffness (modulus) which is very close to that of the control one, provides an additional strong evidence of organic layer being mostly removed. A large amount of scatter appears, further emphasizes a heterogeneous and porous surface structure. It is believed that the constituents of SiO_2 , ZrO_2 , TiO_2 , K_2O, etc. on the glass surface enable different resistance to corrosion by alkali solutions. The reverse is true in the case of fibre with coating and clay, where the modulus value of the alkali treated sample is apparently reduced. This result is expected, since chemical corrosion or swelling more or less occurring in the remaining polymer coating with clay layer. Overall, the only 1 wt% clay reinforced coating layer is rather alkali-resistant. This enhancement is attributed to the fact that the nanometre-thin sheet-like layers of clays act as obstacles to molecules diffusing towards the fibre surface, extending their path through the coating and, thus, decreasing its permeability to alkali liquids. In summary, the nanostructuring coatings show promising potential in nano-defect repair and surface functionalisation for many different applications.

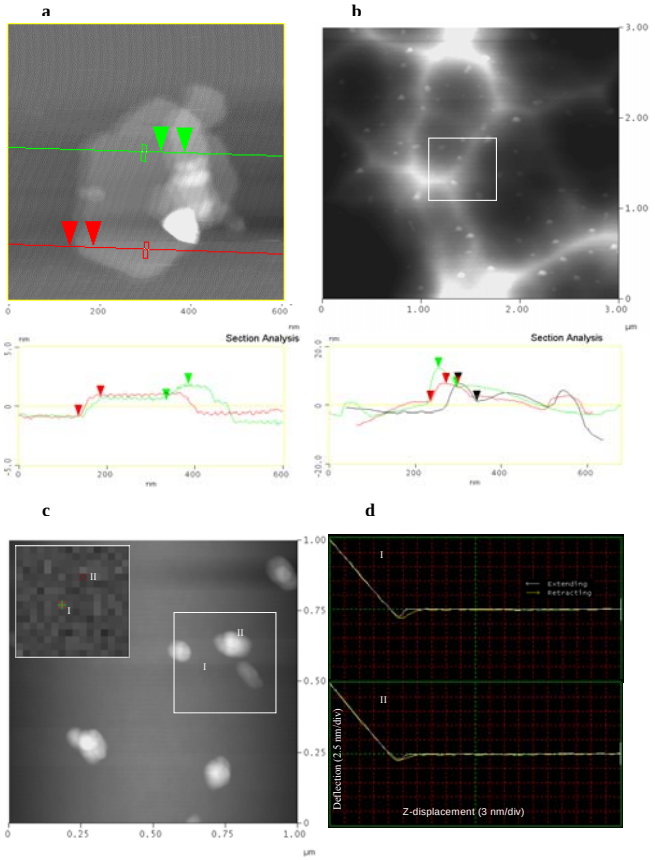

Figure 3: Layered silicate clay and fibre surface coating with clay particles. a-b, AFM topography and section analysis of layered silicate clay and fracture surface of coating with clay after alkali treatment. c-d, AFM topography of clay on fibre surface after pyrolysis treatment. The insert shows the force volume image in the square region. Also shown are cantilever deflection (force) vs. Z-displacement curves corresponding to indentation at I and II, respectively.

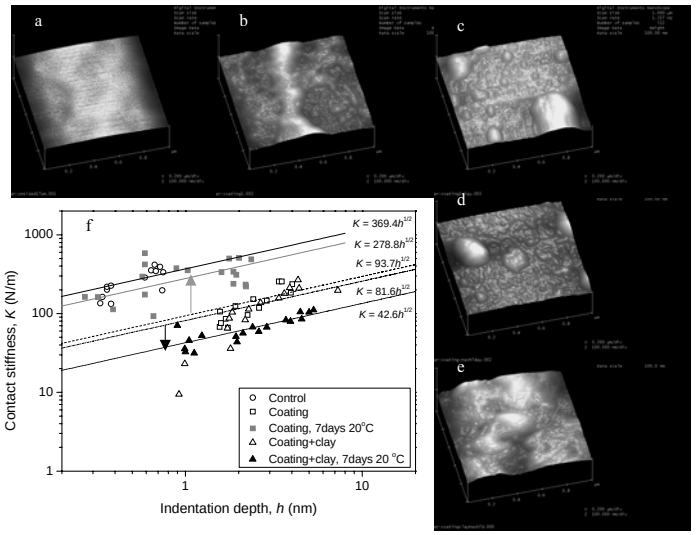

Figure 4: AFM topography images and surface stiffness of AR fibres. a, Control. b-e, Fibre surfaces for coating and coating with nano-clay before and after extracted in 5 wt% NaOH aqueous solution for 7 days in an ambient environment, respectively. f, AFM determination of contact stiffness vs. indentation depth for the silicon tip on the fibre surfaces. The contact stiffness, *K*, is the slope *dF/dh* of the initial elastic unloading curve of nanoindentation test. Variations of the nanoscale surface properties subjected to alkali attack are indicated by the arrows. As a quantitative evaluation of the contact stiffness and modulus of samples, the lines are the best fit to a modified formalism based on equation of Snedden $K = 2\sqrt{2Rh} \cdot E_r$ where R is radius of curvature of indenter tip and ν is Poisson's ratio. E_r is an effective reduced elastic modulus which includes contributions from both the specimen and the indenter: $\frac{1}{E_r} = \frac{1-\nu_i^2}{E_i} + \frac{1-\nu_s^2}{E_s}$ The subscripts i and s refer to the properties of the indenter materials and the specimens, respectively

REFERENCES

[1] S.L. Gao, E. Mäder and R. Plonka, Acta Materila, 52, 4745-4755, 2004.

[2] P. Zinck, E. Mäder and J.F. Gerard, J Mater Sci, 36, 1-8, 2001.

[3] S. Tyagi, J.Y. Lee, G.A. Buxton and A. C. Balazs, Macromolecules, 37, 9160-9168, 2004.

[4] S.L. Gao, E. Mäder, A. Abdkader and P. Offermann, Langmuir, 19, 2496-2506, 2003.

[5] H.J. Gao, B.H. Ji, I.L. Jäger, D. Arzt and P. Fratzl, PNAS, 100, 5597-5600, 2003.

[6] H.J. Gao and B.H Ji, Eng. Fract. Mech., 70, 1777-1791, 2003.